Journal of Marine Research, 56, 75–86, 1998

Linear theory of the effect of a sloping boundary on circulation in a homogeneous laboratory model

by Ross W. Griffiths[1] and George Veronis[2]

ABSTRACT

Griffiths and Veronis (1997) reported observations of the effect of a sloping boundary on the circulation in a sliced-cylinder model of wind-driven circulation in which the flow is driven by the relative rotation of the top lid. A summary of observations for the nearly linear case is given here along with the linear analysis based on the theory of a rotating homogeneous fluid. Good agreement between the two is obtained, and the (straightforward) physics of the system is described.

1. Introduction

Griffiths and Veronis (1997; hereafter, GV) reported experimental observations of the effects of a sloping side boundary on the circulation of a homogeneous fluid in the sliced-cylinder tank of Griffiths and Kiss (1998), when the top lid rotates with angular velocity, $\Omega + \Delta\Omega$, slightly different from that of the cylinder. A perspective diagram of the experimental basin is shown in Figure 1. The bottom has a constant slope of 0.1 relative to the horizontal; the topographic beta effect makes the shallow end simulate north and the deep end south as shown in the figure. The depth is constant along west-east lines. The side walls are the parts of a 45° cone between the (upside down) base of the cone at the top and the intersection of the side of the cone with the sloping bottom. Contours of constant depth are indicated by circles near the rim and D-shaped contours made up of partial circles on the slope and straight (east-west) lines across the interior. The working fluid beneath the circular lid of radius $a = 48.65$ cm has a mean depth of $H_o = 12.5$ cm. The ellipse along which the sloping side wall intersects the bottom is given by

$$r_e = \frac{a - H_o}{1 - \tan\alpha \sin\theta} \tag{1.1}$$

where a is the radius of the rim, H_o the mean depth, α the angle of the sloping bottom and θ the azimuthal angle. The side wall slope is unity, and, because it is a multiplicative constant, does not appear explicitly in r_e.

1. Research School of Earth Sciences, The Australian National University, Canberra 0200 ACT, Australia.
2. Department of Geology and Geophysics, Yale University, P.O. Box 208109, New Haven, Connecticut, 06520-8109, U.S.A.

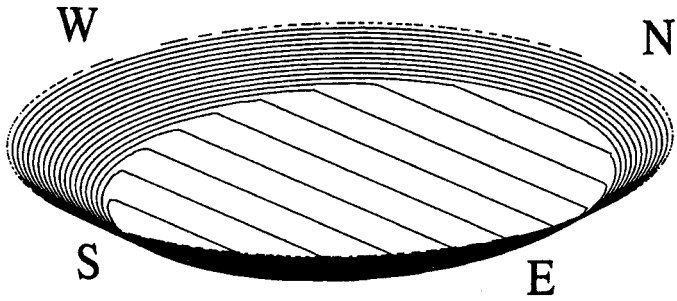

Figure 1. A perspective diagram of the experimental basin with topographically simulated directions corresponding to north, south, east and west as marked. The depth is constant along circles near the rim and on D-shaped contours closer to the interior. The two slopes meet along the ellipse joining the corners of the D-shaped contours and given by Eq. (1.1).

Details of the observed flow are given in GV. Here, we note the contrast between the flow in the cylinder with straight side walls (Fig. 2) and that in the cylinder with sloping walls (Fig. 3). Instead of all interior flow emanating from and returning to a frictionally controlled western boundary layer (Fig. 2), the sloping side generates an interior flow with streamlines that are westward but with a northward drift (Fig. 3). The effect of frictional

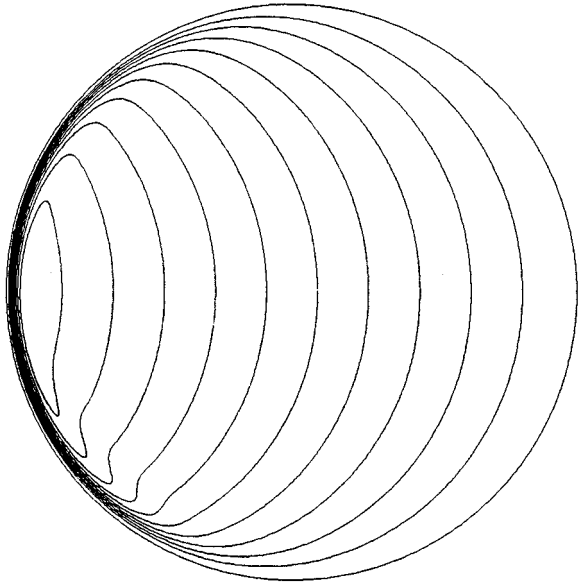

Figure 2. A streamfunction plot showing the steady cyclonic flow computed from a numerical model of the laboratory experiment with vertical side walls (Griffiths and Kiss, 1998). Nonlinear effects cause the small overshoots as the flow emerges from the western boundary layer in the southwest. Cyclonic lid forcing, $R_o = 0.004$, $E = 3.15 \times 10^{-5}$, aspect ratio $H_o/2a = 0.125$.

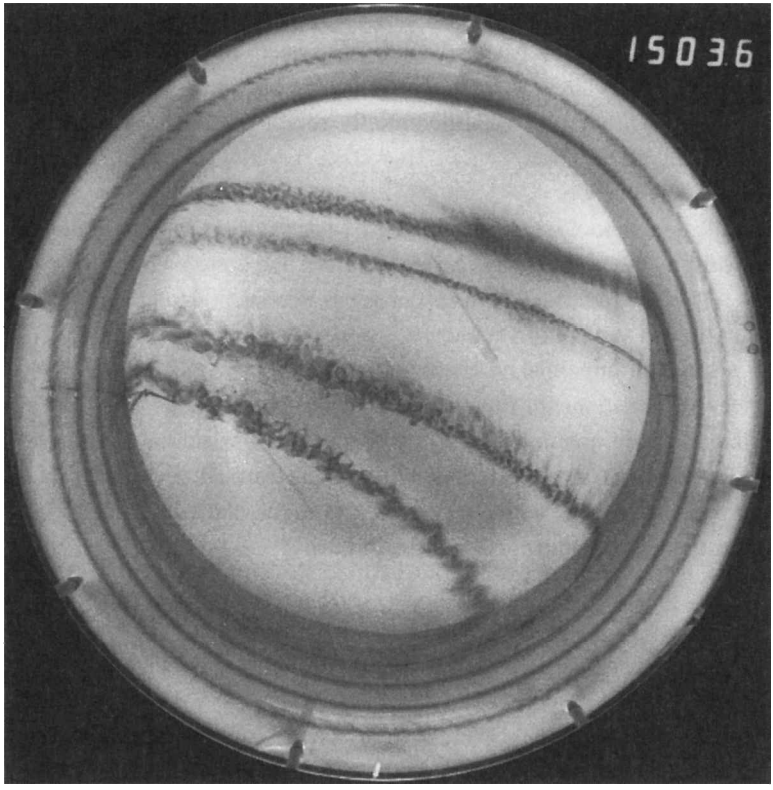

Figure 3. Photograph of the streamlines in the sloping wall case revealed by advection of dye in the steady flow produced by cyclonic forcing with $\Omega = 2$ rad s^{-1}, $E = 3.15 \times 10^{-5}$, $R_o = 0.004$.

dissipation on the slope allows fluid columns to cross depth contours; that occurs on the *eastern* side of the basin.

We had intended to include in GV a theoretical analysis of the flow for the linear case but had made an error which has since been corrected; the corrected theory follows. This paper should be read as part of GV.

2. The mathematical model and its solution

The linear analysis for this flow is relatively simple and the physics that determines the flow is easy to understand. The equations for the conservation of momentum and mass for a homogeneous fluid in a rotating system are

$$\frac{D\mathbf{v}}{Dt} + 2\Omega \times \mathbf{v} = -\frac{1}{\rho}\nabla p + \nu\nabla^2\mathbf{v}, \tag{2.1}$$

$$\nabla \cdot \mathbf{v} = 0, \tag{2.2}$$

where Ω is the angular velocity of rotation of the system, $\mathbf{v}$ is the velocity vector, and ν is kinematic viscosity. Gravity is not relevant in this system because there is no free surface since the homogeneous fluid in our experiment is completely contained between the sloping sides and bottom and the differentially rotating lid. The assumption of linear, steady flow eliminates the term, $D\mathbf{v}/Dt$. Therefore, the flow is determined by geostrophic balance modified by friction.

The theoretical methodology for dealing with such a system, where friction is coupled to geostrophic flow by means of Ekman layers at the top and bottom boundaries, dates back to Greenspan and Howard (1963). More complete accounts, including the treatment of spatially variable top and bottom boundaries, were developed by Greenspan (1968) and by Howard in a series of unpublished lectures that he gave in Stockholm in 1969. Pedlosky (1987) derives the equations for flows under oceanic conditions.

The system is made nondimensional by scaling the horizontal coordinates by a, the vertical by H_o, the horizontal velocities by $a\Delta\Omega$, the vertical velocity by $H_o\Delta\Omega$ and the pressure by $\rho a^2\Omega\Delta\Omega$. Then with $D\mathbf{v}/Dt = 0$, the horizontal part of (2.1) in rectangular cartesian coordinates takes the nondimensional form

$$2\mathbf{k} \times \mathbf{v} = -\nabla p + E_a\nabla^2\mathbf{v} + E\frac{\partial^2\mathbf{v}}{\partial z^2}, \tag{2.3}$$

where $E_a = \nu/\Omega a^2$ and $E = \nu/\Omega H_o^2$.

The procedure for the linear problem is to divide the variables into two parts: (a) a part valid in the Ekman boundary layers near the top and bottom boundaries and decaying rapidly to zero with distance from each boundary, and (b) a (vertically) interior part with zero vertical derivative and valid throughout the depth of the fluid. Boundary conditions at the top and bottom are satisfied by the sum of the two parts. Each part is expanded in powers of $E^{1/2}$ and a set of equations (coefficients of $E^{n/2}$, $n = 0, 1, 2, \ldots$) is derived. The result is that the vertically interior equations at $O(E^0)$ and $O(E^{1/2})$ are geostrophic and satisfy the Taylor-Proudman theorem (zero z derivatives). Since $\partial w/\partial z$ vanishes in the interior at $O(E^0)$ and $O(E^{1/2})$, interior w at the top equals interior w at the bottom. The latter contains a contribution from the sloping bottom. The total normal velocity vanishes at the two boundaries. We make use of that and the Ekman layer solutions to match the vertical velocities of the boundary layers evaluated at the boundaries. The result is expressed in terms of the interior vertical vorticity as

$$\frac{(c+1)}{2}E^{1/2}\zeta + u_n\frac{\partial b}{\partial n} = E^{1/2}, \tag{2.4}$$

where ζ is the vertical vorticity, $b(x, y)$ is the height of the bottom above a reference level, and n denotes the direction toward contours of decreasing depth (increasing b). $c = 2^{1/4}$ over the side walls where the slope is unity and $c \approx 1$ over the gentler slope (0.1) of the interior.

Inside the ellipse where the bottom slope is small the topographic term is $0.1v$ and (2.4) takes the form (u is eastward and v is northward)

$$E_a^{1/2}\left(\frac{\partial v}{\partial x}-\frac{\partial u}{\partial y}\right)+0.1v=E_a^{1/2}, \tag{2.5}$$

or in terms of the pressure

$$E_a^{1/2}\nabla^2 p+0.1\frac{\partial p}{\partial x}=2E_a^{1/2}. \tag{2.6}$$

Between the ellipse and the rim the Ekman pumping velocity must be corrected because the slope (=1) is not small. Pedlosky (1987, Eq. 4.9.32) gives the form of w with that correction and the vorticity equation in this case becomes (the velocity, v^r, is radial and v^θ is azimuthal)

$$\frac{E^{1/2}}{2}\left[(\cos^{-1/2}\alpha+1)\frac{1\partial(rv^\theta)}{r\partial r}-(\cos^{-5/2}\alpha+1)\frac{1\partial v^r}{r\partial\theta}\right]+v^r\tan\theta=E^{1/2}, \tag{2.7}$$

or in terms of the pressure in polar coordinates and with $\alpha=\pi/4$,

$$\frac{E^{1/2}}{2}\left[(2^{1/4}+1)\frac{1}{r}\frac{\partial\left(r\dfrac{\partial p}{\partial r}\right)}{\partial r}+(2^{5/4}+1)\frac{1}{r^2}\frac{\partial^2 p}{\partial\theta^2}\right]-\frac{1\partial p}{r\partial\theta}=E^{1/2}. \tag{2.8}$$

The change from E_a in (2.5) to E in (2.7) is due to the difference in the aspect ratios in the two regions (inside and outside the ellipse).

a. E^0 (subscript 0) solution

It follows from (2.4) and (2.7) that the lowest order (E^0) flow is parallel to contours of constant depth. Then from (2.7) with $v_o^r=0$ we obtain

$$v_o^\theta=\frac{r}{(2^{1/4}+1)}, \tag{2.9}$$

or

$$p_o=\frac{(r^2-1)}{(2^{1/4}+1)}, \tag{2.10}$$

where $p_o=0$ on $r=1$. A (lateral) boundary layer can be added to make total $v^\theta=0$ on $r=1$. The value of p_o on a specific depth contour inside the ellipse equals the value on the same depth contour over the slope, i.e., p_o is constant on a D-shaped contour. So the values given by (2.10) on the ellipse are extended into the region inside the ellipse. However, because

the interior slope is only a tenth of that in the boundary region, the zonal velocity in the interior is only about a tenth of the azimuthal velocity over the slope.

b. $E^{1/2}$ (subscript 1) solution

From (2.5) the northward velocity within the ellipse occurs at this order and is given by

$$v_1 = 10E_a^{1/2}. \tag{2.11}$$

The contribution from the frictional term in (2.5) is less than one percent of (2.11). In terms of pressure (2.11) yields

$$p_{1x} = 20E_a^{1/2},$$

or

$$p_1 = 20E_a^{1/2}(x - x_b), \tag{2.12}$$

where we use the boundary condition $p_1 = 0$ on the eastern rim where $x = x_b$.

On the sloping boundary we now have to solve (2.8) for p_1. The boundary conditions for that elliptic equation are the value of p_1 given by (2.12) evaluated on the ellipse, $r = r_e$, and $p_1 = 0$ on $r = 1$. The boundary conditions in the θ direction are that p_1 and its derivatives be periodic. The solution for the slope region is obtained by numerical relaxation.

The streamlines (p contours) over the entire domain with p correct to $O(E^{1/2})$ are shown in Figure 4. Observed trajectories for the experiments of GV are depicted in Figure 3. Except for the discontinuous velocities (derivatives of p) where the solutions inside and outside the ellipse come together, the patterns resemble each other.

c. $E^{1/4}$ correction

We have added Stewartson $E^{1/4}$ layers (indicated by primed variables) on each side of $r = r_e$ to eliminate the discontinuity in the azimuthal velocity, v (we drop the superscript θ here), across the ellipse. On the slope side the radial coordinate is stretched by the substitution

$$r - r_e = \eta E^{1/4}, \qquad \eta > 0 \tag{2.13}$$

where $\partial/\partial\eta = O(1)$. The dominant term for Ekman pumping at the top ($z = 1$) is the vertical velocity given by

$$w' = -\frac{E^{1/4}}{2}\frac{\partial v'}{\partial \eta}. \tag{2.14}$$

At the sloping bottom ($z = 1 - r_e$) the Ekman pumping is

$$w' = -\frac{E^{1/4}}{2^{3/4}}\frac{\partial v'}{\partial \eta}. \tag{2.15}$$

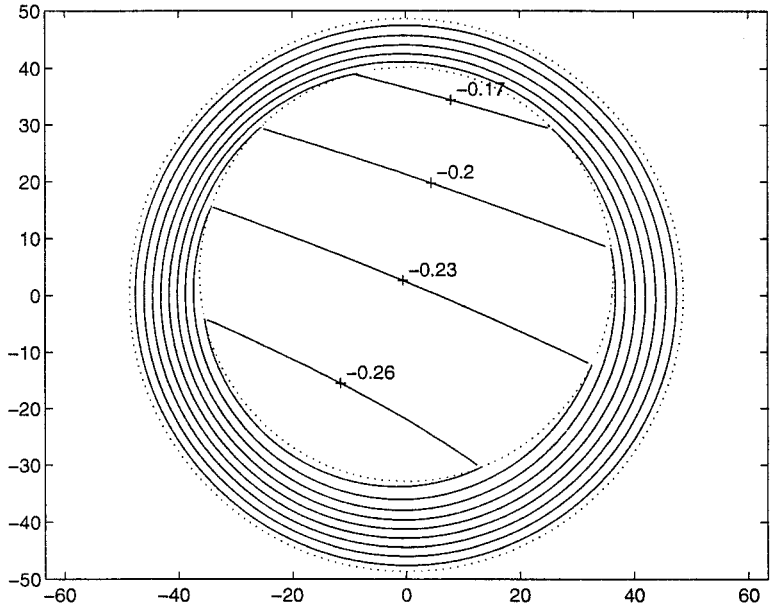

Figure 4. Streamlines (p contours) for the linear ($R_o = 0$) system with contributions of $O(E^0)$ plus $O(E^{1/2})$ over the entire basin with interior and slope region calculated separately but joined by matching values of p along the ellipse. $\Omega = 2$ rad s^{-1}, $E = 3.15 \times 10^{-5}$.

Since w' is quasi-geostrophic and satisfies the equation

$$\frac{\partial^2 w'}{\partial z^2} = 0, \tag{2.16}$$

we choose

$$w' = -\frac{E^{1/4}}{2}\frac{z-(1-r_e)}{1-(1-r_e)}\frac{\partial v'}{\partial \eta} + \frac{E^{1/4}}{2^{3/4}}\frac{1-z}{1-(1-r_e)}\frac{\partial v'}{\partial \eta}, \tag{2.17}$$

which satisfies conditions (2.14) to (2.16).

The continuity equation in the $E^{1/4}$ layer takes the form (note that the depth can be considered constant inside the $E^{1/4}$ layer)

$$E^{-1/4}\frac{\partial u'}{\partial \eta} + \frac{\partial w'}{\partial z} = 0, \tag{2.18}$$

where u' is the radial velocity and where we neglect θ derivatives. Eq. (2.18) admits a streamfunction defined by

$$E^{-1/4}u' = \frac{\partial \psi}{\partial z}, \qquad w' = -\frac{\partial \psi}{\partial \eta}. \tag{2.19a,b}$$

Eqs. (2.17) and (2.19b) are satisfied by

$$\psi = \left[\frac{E^{1/4}}{2}\frac{z-(1-r_e)}{1-(1-r_e)} - \frac{E^{1/4}}{2^{3/4}}\frac{1-z}{1-(1-r_e)}\right]v', \tag{2.20}$$

and use of (2.19a) yields

$$2u' = \frac{E^{1/2}}{r_e}(1+2^{1/4})v'. \tag{2.21}$$

Since the $E^{1/4}$ azimuthal velocity satisfies the equation

$$E^{1/2}\frac{\partial^2 v'}{\partial \eta^2} - 2u' = 0, \tag{2.22}$$

we end up with the differential equation for v',

$$\frac{\partial^2 v'}{\partial \eta^2} - \frac{1+2^{1/4}}{r_e}v' = 0, \tag{2.23}$$

which has the solution

$$v' = c\exp\left[-\left(\frac{1+2^{1/4}}{r_e}\right)^{1/2}\eta\right], \tag{2.24}$$

where c is to be determined by matching total v across r_e. An analogous procedure as $r \to r_e$ from inside the ellipse yields

$$v' = d\exp\left[-\left(\frac{2}{1-0.1r_e}\right)^{1/2}\zeta\right], \tag{2.25}$$

where $r_e - r = \zeta E_a^{1/4}$, $\zeta > 0$ and d must also be determined.

If we denote the $E^0 + E^{1/2}$ azimuthal velocity over the slope without the $E^{1/4}$ correction by v^s and that inside the ellipse by v^i, we can match the total azimuthal velocities and the pressures from the two regions at $r = r_e$ to obtain

$$d = c + v^s - v^i, \tag{2.26}$$

and

$$c = \frac{v^i - v^s}{1 + \left[\frac{r_e}{1+2^{1/4}}\frac{2}{1-0.1r_e}\frac{a}{H_o}\right]^{1/2}}. \tag{2.27}$$

The pressure field including the $O(E^{1/4})$ contribution is continuous with continuous velocities (derivatives) and appears in Figure 5 for $E = 3.15 \times 10^{-5}$. The qualitative

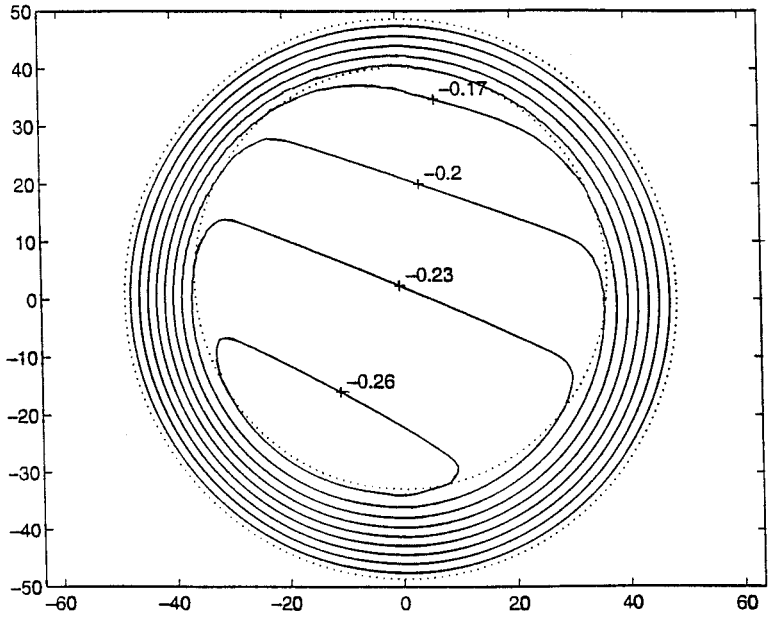

Figure 5. Streamlines (p contours) for the same system as in Figure 4 but with $O(E^{1/4})$ corrections to match values of p and v across the ellipse so that the discontinuities in velocity of Figure 4 are eliminated.

agreement with experiment is pretty good, though the observed field has more curvature in the interior of the basin.

This linear solution gives surprisingly good quantitative results for the velocities. The northward velocity in the interior appears in (2.11) and for the case calculated above gives $v/a\Delta\Omega = 0.0145$ which agrees with the measured values to within 1%. (The experiments yielded a value of v that is largely independent of R_o.) It would appear from Figure 6a that the calculated zonal velocity is smaller than the observed. However, the experiments generally showed a consistent increase in zonal velocity with increasing R_o whereas Figure 6a indicates a decrease as R_o increases from 0.004 to 0.008. The motion is so slow for $R_o = 0.004$ that we have to consider the measured values of u (note the large scatter) to be unreliable. From our observation that u increases with increasing R_o we expect the correct observed values to lie just above the (more easily measured) ones for $R_o = 0.008$ in Figure 6a and that would bring them very close to the calculated values. Over the slope at midlatitude, theory and observations of the azimuthal velocity agree very well, as seen in Figure 6b.

All of these comparisons are made for an experiment with $R_o = 0.004$, the smallest value that enabled us to avoid spurious effects due to convection and resulting density stratification. The criterion that the flow be linear is that R_o be much smaller than $E^{1/2}$, which in this case is 0.0056, so even for $R_o = 0.004$ nonlinear effects in the experiment are not

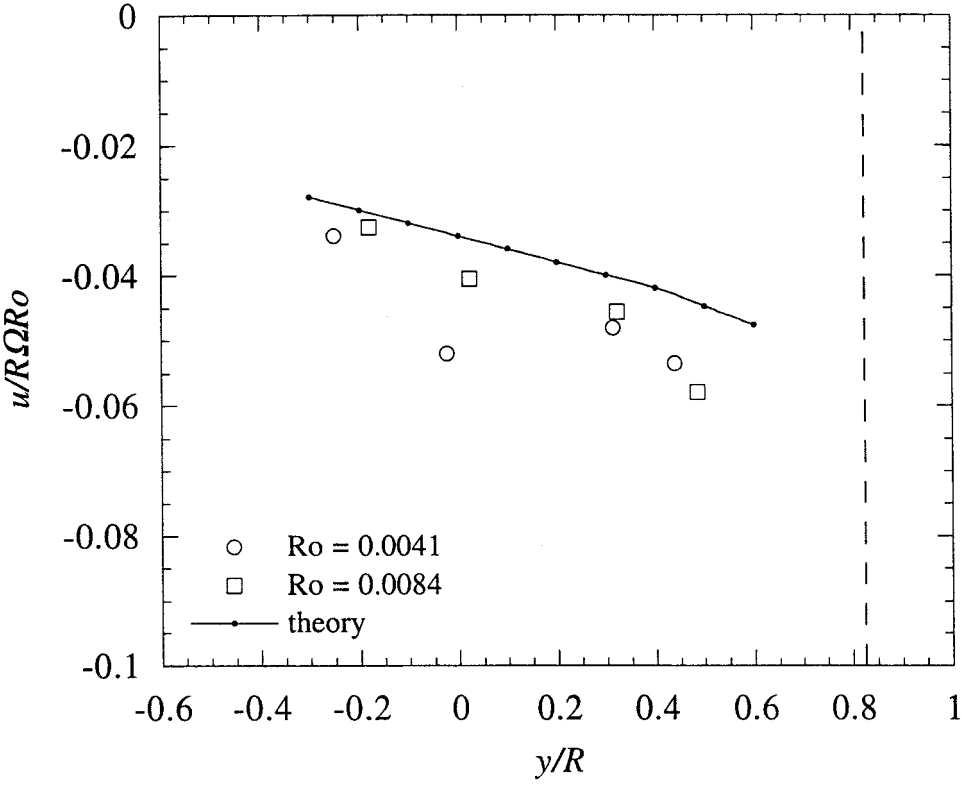

Figure 6. (a) Calculated and observed zonal (u) velocities as functions of y along $x = 0$. (b) Calculated and observed meridional (v) velocities as functions of x along $y = 0$.

negligible. Support for that conclusion comes also from the numerical experiment for the vertical wall case shown in Figure 2 where the observed overshoot is due to nonlinearity.

3. Discussion

Physically, the system is completely consistent with expected dynamical behavior when the lid is forced with positive relative vorticity. A column of fluid starting off at the southeast extremity of its trajectory in the interior is driven northward by the imposed positive vorticity and it moves westward (because of the basic flow along D-shaped contours) to arrive at a point at the northwest extremity. Along this trajectory it has acquired positive potential vorticity (a positive value of f/H, i.e., a decreasing value of H) from the rotating lid. It then joins smoothly (no change in depth) onto the slope and is driven anticlockwise along the constant depth contour at which it entered the slope region until it reaches the vicinity of the point at which it originated. During this anticlockwise motion on the slope the Ekman transport toward the rim generated at the top of the column is exactly balanced by the inward Ekman layer transport along the bottom. The geostrophic

Griffiths & Veronis: Sloping boundary 85

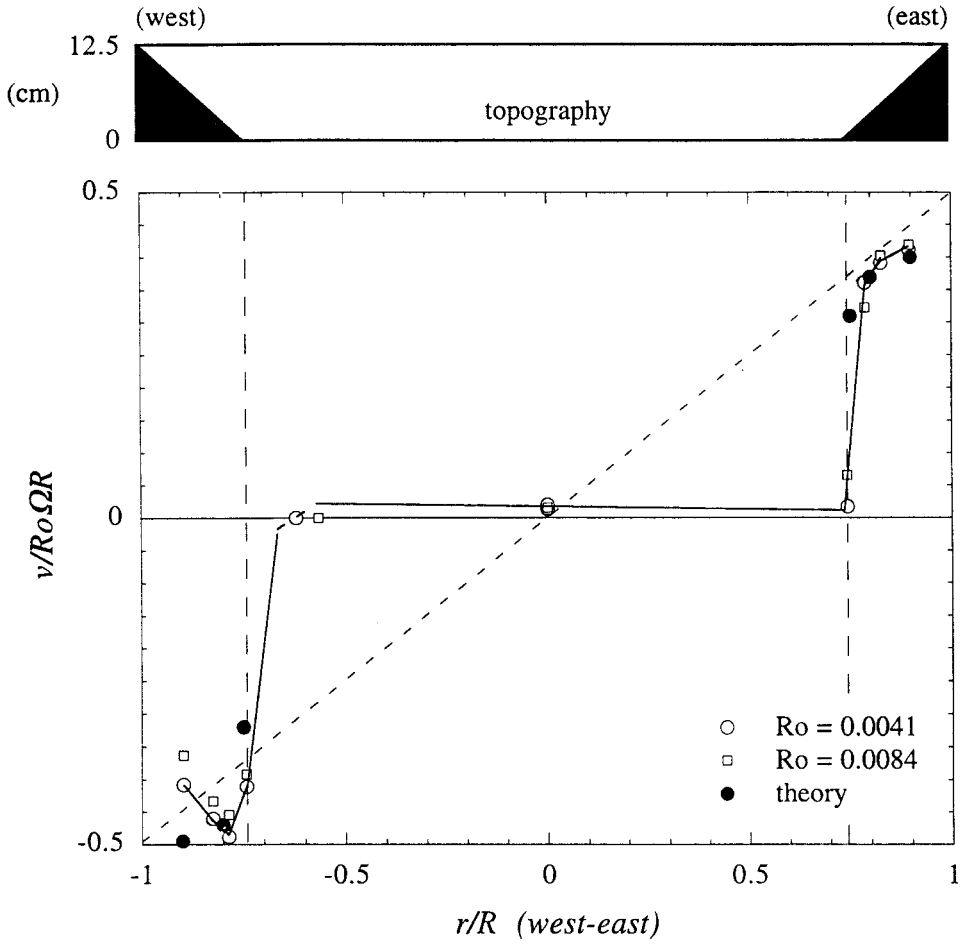

Figure 6. (Continued)

column then turns inward toward the interior and in the process crosses depth contours while dissipating the positive vorticity that it acquired from the lid while crossing the interior. As it descends the slope, it lengthens until it reaches its original column depth.

One difference between this flow and the more familiar one in the tank without a slope is that most of the effective dissipation takes place here on the eastern side rather than along a western boundary layer. The physical balances are the same, but the fluid column takes advantage of the geostrophic contour to move inviscidly to the south and east before dissipation sets in. The slope provides a short-circuit path by which a particle of fluid is delivered from the point where it has maximum potential vorticity to the region where it can dissipate that vorticity and regain its initial position and depth. There is no comparable region in the model with vertical walls or in the traditional wind-driven ocean circulation

model on the beta plane, where a column of fluid starts dissipating the vorticity that it has acquired as soon as it reaches the point where the vorticity is a maximum.

However, addition of side wall topography to the oceanic model provides a path that can function in a manner similar to the one encountered here. Salmon (1992) derived a result similar to ours for a model of ocean circulation with a slope along the western boundary. In his case the dissipation region was at the southwestern corner where flow coming in from the north is turned around and delivered to a lower latitude. All of the dissipation in his case takes place in that southwestern corner where the initial value of the potential vorticity is restored before the column exits the corner. Apart from the different geometry our model and his behave in exactly the same way. The implication for ocean circulation is that the dissipation of the vorticity input by the wind may take place in regions far removed from the ones traditionally assumed. The actual geometry of the topography will determine where that takes place.

The foregoing theory is based on the assumption that the flows in the interior of the basin and over the slope can be analyzed separately and that the two can be joined to give a complete solution by matching along the ellipse dividing the two regions. A check on this procedure can be obtained as part of a numerical solution of the entire region which is currently being carried out.

Acknowledgments. We are indebted to Rick Salmon, who argued convincingly that the original numerical solution contained an error, and to Philip Bogden, who wrote the graphics program for Figures 5 and 6. The work was partly supported by the National Science Foundation through grant OCE 9312523.

REFERENCES

Greenspan, H. P. 1968. The Theory of Rotating Fluids, Cambridge University Press, 327 pp.

Greenspan, H. P. and L. N. Howard. 1963. On a time-dependent motion of a rotating fluid. J. Fluid Mech., *17,* 385–404.

Griffiths, R. W. and A. E. Kiss. 1998. Flow regimes in a wide 'sliced-cylinder' model of homogeneous ocean circulation. J. Fluid Mech. (submitted).

Griffiths, R. W. and George Veronis. 1997. A laboratory study of the effects of a sloping side boundary on wind-driven circulation in a homogeneous ocean model. J. Mar. Res., *55,* 1103–1126.

Pedlosky, J. 1987. Geophysical Fluid Dynamics, Springer-Verlag, 710 pp.

Salmon, R. L. 1992. A two-layer Gulf Stream over a continental slope. J. Mar. Res., *50,* 341–361.

Received: *1 December, 1997.*